BBAA VI International Colloquium on:
Bluff Bodies Aerodynamics & Applications
Milano, Italy, July, 20–24 2008

CROSSWIND STABILITY OF HIGH-SPEED TRAINS: A STOCHASTIC APPROACH

Christian Wetzel[⋆] **and Carsten Proppe**[⋆]

[⋆]Institut für Technische Mechanik
Universität Karlsruhe, Kaiserstr. 10, 76131 Karlsruhe, Germany
e-mails: proppe@itm.uka.de, wetzel@itm.uka.de

Keywords: crosswind stability, high-speed trains, stochastic analysis, gust model, importance sampling, sensitivity analysis

Abstract The modern developments in railway engineering have been showing a trend to faster and more energy efficient trains with a higher capacity of passenger transportation. These efforts are directly leading to light-weight cars with distributed actuation. Unfortunately these developments are in contrast to a save use in strong crosswind conditions. Consequently, crosswind stability has become a crucial issue of modern railway vehicle design that cannot be solved easily, because counter-measures are very expensive.
Sufficient crosswind stability is also an important criterion in the approval process of railway vehicles. In many countries, the approval process foresees stability predictions based on worst case scenarios, where uncertainties are taken into account by means of safety factors and comparison with reference vehicles. This procedure is a burden for innovations and hinders the interoperability of railway vehicles. Therefore, in recent years probabilistic methods have been proposed, some of which are already common design criteria in other fields of engineering, e.g. for wind turbines. A method to compute the reliability of railway vehicles under strong crosswind is presented. In consideration of the given stochastic wind excitation the response of a train model and the corresponding probability of failure have been computed. The major failure criterion to determine the reliability is the lowest wheel-rail contact force of the railway vehicle.
In order to isolate the most influential random variables and to quantify the influence of design parameters, a sensitivity analysis has been undertaken.

1 INTRODUCTION

This investigation is focused on a detailed quantification of the probability of overturning for a railway vehicle and applies a wind gust model that has been proposed for the fatigue analysis of wind turbines [1, 2]. Two wind scenarios are investigated: a train coming out of a tunnel immediately being hit by a gust and a train traveling on an embankment under constant mean wind load being hit by a gust, respectively. In a second step, sensitivity analyses with respect to the stochastic excitation variables and with respect to deterministic design parameters are performed and the most crucial variables are accentuated. Similar investigations have been carried out previously in [3]. However, this study differs from previous works by the environmental model, especially the gust model, the stochastic analysis techniques and the way the sensitivities are computed.

Figure 1: Train which turned over during winter storm Kyrill in January 2007, courtesy of Schweizer Fernsehen-Schweiz Aktuell

2 AERODYNAMIC CONSIDERATIONS

In this section the wind model, which is used in this work is presented. The turbulent wind loads on the railway vehicle, the used gust characteristics and three different crosswind scenarios are introduced. Two of the three scenarios are so called artificial gust models and the remained third wind characteristic is a pure turbulent wind process without any additional gusts. First some common aerodynamic assumptions concerning the atmospheric wind are introduced. The wind component u is blowing in direction of the x-axis and consists of a mean wind $u_{_0}$ and a small turbulent, zero-mean velocity component u'. For simplicity and because of their small magnitude compared to the component u the vertical and horizontal turbulent wind components v' and w' are not considered in this work.

2.1 Mean wind

The averaged flow involving friction in the atmospheric boundary layer can be described as a function of the height z above ground by the logarithmic-law

$$u_{_{0}10}(z) = k_{_T} u_{_{0}10}(10[m]) \ln\left(\frac{z}{z_{_0}}\right), \tag{1}$$

where the wind velocity $u_{_{0}10}(z)$ is the the 10-minute mean wind, $u_{_{0}10}(10[m])$ is the reference velocity at a height of 10 metres and $z_{_0}$ and $k_{_T} = 0.19\left(\frac{z_{_0}}{0.05}\right)^{0.07}$ are parameters describing the roughness of the terrain, [8]. The probability distribution of the mean wind velocity at different land sites can often be described with good accuracy by a Rayleigh distribution.

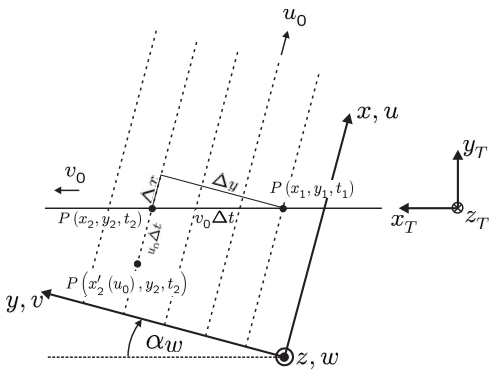

Figure 2: Fixed and moving coordinate system of the wind velocity and railway vehicle

2.2 Turbulence

The longitudinal turbulent wind velocity u at a fixed point in the atmospheric boundary layer can be described by the von Karman power spectral density (PSD)

$$S_{u'u'}(f) = \frac{4\sigma_{u'}^2 L_{u'x}}{u_0 \left(1 + 70.8 \left(\frac{f L_{u'x}}{u_0}\right)^2\right)^{\frac{5}{6}}} \tag{2}$$

where the variance $\sigma_{u'}^2$ and the integral length scale $L_{u'x}$ can be calculated by the equations

$$\sigma_{u'} = \left(1 - 5 * 10^{-5} \left(\log\left(\frac{z_0}{0.05}\right) + 2\right)^7\right) \frac{u_0}{\ln\left(\frac{z}{z_0}\right)} \tag{3}$$

and

$$L_{u'x} = 50 \frac{z^{0.35}}{z_0^{0.063}}, \tag{4}$$

respectively. The turbulent fluctuations of the wind speed are considered to follow a normal distribution with zero mean. This assumption is a very good approximation of the atmospheric wind and it simplifies drastically all calculations on the turbulent wind process. For a vehicle, which is running with a certain speed v_0 through the spatial wind field, the mentioned von Karman PSD has to be modified as described in [9]. According to figure 2 the PSD for the longitudinal wind speed of a moving vehicle yields

$$S_{u'u'}(f) = \left(\frac{4\sigma_{u'}^2 L_{u'}}{v_{res} \left(1 + 70.8 \left(\frac{f L_{u'}}{v_{res}}\right)^2\right)^{\frac{5}{6}}}\right) \left[C_{u'} + (1 - C_{u'}) \left(\frac{0.5 + 94.4 \left(\frac{f L_{u'}}{v_{res}}\right)^2}{1 + 70.8 \left(\frac{f L_{u'}}{v_{res}}\right)^2}\right)\right], \tag{5}$$

with the abbreviations

$$C_{u'} = \left(\frac{v_0}{v_{res}} \sin\alpha_w + \frac{u_0}{v_{res}}\right)^2, \quad L_{u'} = L_{u'x} \sqrt{C_{u'} + (1 - C_{u'}) \frac{4 L_{u'y}^2}{L_{u'x}^2}} \tag{6}$$

and

$$v_{res} = \sqrt{v_0^2 + u_0^2 + 2 u_0 v_0 \sin\alpha_w}. \tag{7}$$

The ratio $\frac{L_{u'y}}{L_{u'x}}$ of the integral length scales lies between 0.42 and 0.3 and is set to 0.35 according to [10].

2.3 Wind-load

The wind excitation on the railway vehicle is modeled as a concentrated wind load which can be described by the characteristic equation

$$F = \frac{1}{2}\rho_L A_F C_W \left(u_0 + u'\right)^2 \text{ sign}(u_0 + u'), \tag{8}$$

where the variables ρ_L, A_F and C_W are the density of air, a characteristic area and the aerodynamic coefficient. The aerodynamic coefficients are different for every kind of vehicle and have to be determined by experiments in wind-tunnels or by computational fluid dynamics (CFD). These coefficients are not deterministic variables but have inherent uncertainties and therefore are treated as stochastic variables, which follow a normal distribution with a standard deviation of 10% of the mean value. Unfortunately, sophisticated wind effects, as e.g. vortex shedding can not be described by such an approach. To consider vortex shedding a common extension in aeroelasticity is, to expand the aerodynamic coefficients in a series with harmonic fluctuating coefficients. With such an approach it is possible to take the superelevation of the lift forces of a railway vehicle into account.

Strictly speaking equation 8 is not correct for a vehicle with a spatial dimension because for

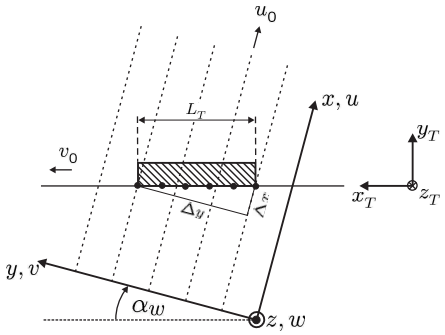

Figure 3: Spatial object in the wind velocity field

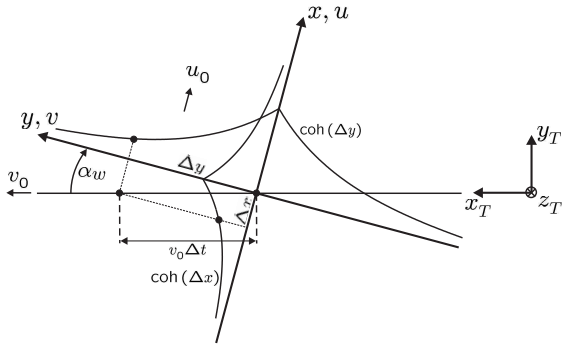

Figure 4: Spatial characteristic of the coherence gust model

such an object a spatial averaging of the squared wind velocity has to be done as shown in the following equation:

$$F(t) = \frac{1}{2}\rho_L A_F C_W \left(u_0^2 + 2\frac{u_0}{A_F}\int_{A_F} u'(x,y,z,t)dA_F + \frac{1}{A_F}\int_{A_F} u'^2(x,y,z,t)dA_F\right). \tag{9}$$

The simulation of such a spatial averaged, squared wind velocity is numerically demanding because a spatial and time dependent wind field has to be generated and then an averaging procedure has to be done in every time step. A possibility to circumvent this complexity is to look at the wind force in the frequency domain. After calculating the correlation function

$$\begin{aligned} R_{FF}(\tau) &= \\ &= \left(\frac{\rho_L A_F C_W}{2}\right)^2 \left[\left(u_0^2 + \sigma_{u'}^2\right)^2 + 4\frac{u_0^2}{A_F^2}\int_{A_F}\int_{A'_F} R_{u'u'}(x,y,z,x',y',z',\tau)dA_F\, dA'_F \right. \\ &+ \left. \frac{2}{A_F^2}\int_{A_F}\int_{A'_F} R_{u'u'}^2(x,y,z,x',y',z',\tau)dA_F\, dA'_F\right], \end{aligned} \tag{10}$$

it is straight forward to determine the PSD

$$\begin{aligned} S_{FF}(f) &= \\ &= \left(\frac{\rho_L A_F C_W}{2}\right)^2 \left[\left(u_0^2+\sigma_{u'}^2\right)^2 \delta(f) + 4\frac{u_0^2}{A_F^2}\int_{A_F}\int_{A'_F} S_{u'u'}(x,y,z,x',y',z',f)dA_F\,dA'_F \right. \\ &+ \left. \frac{2}{A_F^2}\int_{A_F}\int_{A'_F}\int_{-\infty}^{\infty} S_{u'u'}(x,y,z,x',y',z',\alpha)S_{u'u'}(x,y,z,x',y',z',f-\alpha)d\alpha\,dA_F\,dA'_F\right]. \end{aligned} \tag{11}$$

by Fourier-transformation of the correlation function. Neglecting the phase angle of the coherence function coh (x,y,z,x',y',z',f) the cross spectral density

$$S_{u'u'}(x,y,z,x',y',z',f) \approx \text{coh}\,(x,y,z,x',y',z',f)\,S_{u'u'}(f) \tag{12}$$

can be substituted into equation 11. In the resultant equation

$$\begin{aligned} S_{FF}(f) &= \left(\frac{\rho_L A_F C_W}{2}\right)^2 \left[\left(u_0^2+\sigma_{u'}^2\right)^2 \delta(f)\right. \qquad (13)\\ &+ 4\frac{u_0^2}{A_F^2}\int_{A_F}\int_{A'_F}\text{coh}(x,y,z,x',y',z',f)dA_F\,dA'_F\;S_{u'u'}(f) \\ &+ \frac{2}{A_F^2}\int_{-\infty}^{\infty}\left\{S_{u'u'}(\alpha)S_{u'u'}(f-\alpha)\right. \\ &\cdot \left.\left.\int_{A_F}\int_{A'_F}\text{coh}(x,y,z,x',y',z',\alpha)\,\text{coh}(x,y,z,x',y',z',f-\alpha)dA_F\,dA'_F\right\}d\alpha\right]. \end{aligned}$$

the terms

$$\chi^2(f) = \frac{1}{A_F^2}\int_{A_F}\int_{A'_F}\text{coh}(x,y,z,x',y',z',f)dA_F\,dA'_F \tag{14}$$

and

$$\chi^2_{nl}(\alpha,f) = \frac{1}{A_F^2}\int_{A_F}\int_{A'_F}\text{coh}(x,y,z,x',y',z',\alpha)\,\text{coh}(x,y,z,x',y',z',f-\alpha)dA_F\,dA'_F \tag{15}$$

are called linear and nonlinear admittance functions, respectively. The coherence function is often approximated by the exponential function

$$\text{coh}\,(x,y,z,x',y',z',f) = \exp\left\{-\sqrt{\left(\frac{C_{u'x}f\Delta x}{u_0}\right)^2+\left(\frac{C_{u'y}f\Delta y}{u_0}\right)^2+\left(\frac{C_{u'z}f\Delta z}{u_0}\right)^2}\right\}. \tag{16}$$

Corresponding to figure 3 using the transformations $\Delta x = \Delta x_T \sin\alpha_w$, $\Delta y = \Delta x_T \cos\alpha_w$ and $\Delta z = \Delta z_T$ the coherence function can be determined to

$$\text{coh}\,(\Delta x_T,\Delta z_T,f) = \exp\left\{-\frac{|f|}{u_0}\sqrt{\Delta x_T^2\left[(C_{u'x}\sin\alpha_w)^2+(C_{u'y}\cos\alpha_w)^2\right]+(C_{u'z}\Delta z_T)^2}\right\}. \tag{17}$$

As shown in [11] the computation of the linear admittance function can be reduced to the 2-dimensional integral

$$\chi^2(f) = \frac{4}{L_T^2 H_T^2}\int_0^{L_T}\int_0^{H_T}(L_T-x_T)(H_T-z_T)\,\text{coh}(x_T,z_T,f)dz_T\,dx_T. \tag{18}$$

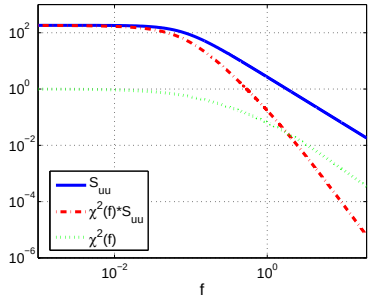

Figure 5: Von Karman PSD, von Karman PSD with linear admittance function and linear admittance function.

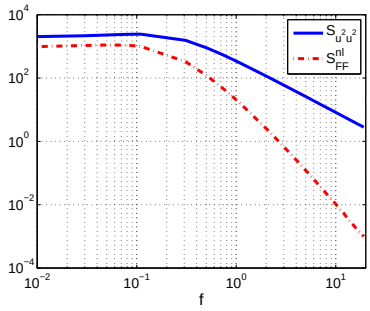

Figure 6: Nonlinear part of PSD $S_{FF}(f)$ with and without nonlinear admittance function $\chi^2_{nl}(\alpha, f)$.

This reduction is also possible for the nonlinear admittance function but in this case an additional integration about the frequency α has to be done. The very advantage of the stated proposal is the easy simulation of the averaged wind force by a spectral decomposition scheme using the von Karman PSD and the vehicle specific admittance functions.

2.4 Gust-characteristic

Gust scenarios are utilized to model certain extreme wind conditions without needing to wait for an occurrence in the normal turbulent wind process. All the gusts with their amplitudes and durations are present in the von Karman PSD but the probability of occurrence for such extreme events is very low and so long simulation runs have to be performed to get high amplitudes. A gust in this sense is defined as the maximum deviation in wind speed between two consecutive mean wind crossings. A recently proposed method where an artificial gust scenario can be superposed to the turbulent fluctuations is the so called constrained-simulation approach which has been developed for wind turbine reliability calculations, [2]. The major advantage of this method is, that the turbulent wind process with the superimposed gust characteristic is statistically indistinguishable from the wind process without the artificial gust. In the resultant equation for the constrained wind velocity

$$u(t) = (u_0 + u'(t)) + \rho_{u'u'}(t - t_B)(A - u'(t_B)) - \frac{\dot{\rho}_{u'u'}(t - t_B)\,\dot{u}'(t_B)}{\ddot{\rho}_{u'u'}(t_B)}, \tag{19}$$

the second term generates a gust at time t_B with a certain amplitude A and the third term makes sure, that at t_B the gust is really a maximum. The function $\rho_{u'u'}(t)$ in equation 19 is the normalized correlation function and the relation $\dot{\rho}_{u'u'}(0) = 0$ should hold to fulfill the stated conditions. A disadvantage of using the correlation function as gust characteristic lies in its frequency independence. This makes it impossible to simulate gusts with different durations. A way out of this is to use the coherence function instead, as it is referred to as being a narrow band correlation function and so has a frequency dependence. After mapping the coherence function on the time domain, according to figure 4, the resultant wind velocity can be given

$$u(t) = (u_0 + u'(t)) + u^*_B(t - t_B)(A - u'(t_B)) - \frac{\dot{u}^*_B(t - t_B)\,\dot{u}'(t_B)}{\ddot{u}^*_B(t_B)}, \tag{20}$$

with the gust characteristic

$$u^*_B(t) = \exp\left\{-\frac{1}{2Tu_0}\sqrt{(C_{u'x}v_0\Delta t\sin\alpha_w + u_0\Delta t)^2 + (C_{u'y}v_0\Delta t\cos\alpha_w)^2}\right\}, \tag{21}$$

where the parameter T describes the duration of the gust.
The measured, normalized gust amplitudes $\tilde{A} = \frac{A}{\sigma_{u'}}$ are often fitted by a half gaussian proba-

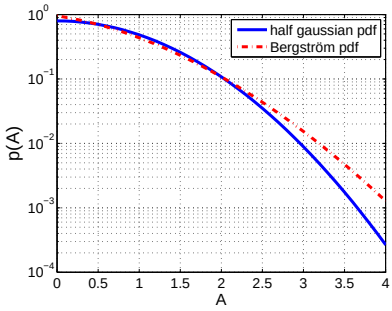

Figure 7: Half gaussian and Bergström probability density functions of gust amplitude $\tilde{A}$

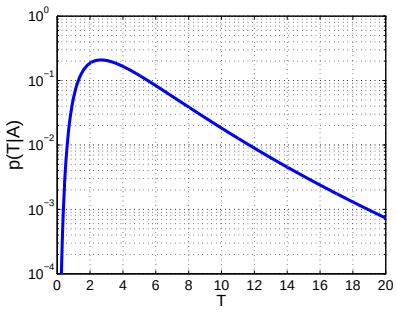

Figure 8: Lognormal probability density function of gust duration $\tilde{T}$

bility density function

$$p(\tilde{A}) = \frac{2}{\sqrt{2\pi}} \exp\left(-\frac{\tilde{A}^2}{2}\right), \tag{22}$$

as has been done in [4]. Bergström [12] obtained from the same experimental data as used in [4] the probability density function

$$p(\tilde{A}) = -\left(2a_1|\tilde{A}| + b_1\right) \exp\left\{a_1\tilde{A}^2 + b_1|\tilde{A}|\right\},\ a_1 = -0.245,\ b_1 = -0.953 \tag{23}$$

which is based on a two parameter fit. In figure 7 the half gaussian and the Bergström probability density functions are shown and it can be seen that for small probabilities (high amplitudes) there is a remarkable difference between both densities, which has a great influence on the failure probabilities. A good approximation of the probability density function of the normalized gust duration $\tilde{T} = \frac{T}{\overline{T}}$ is given in [4], where the data has been fitted to a lognormal density function

$$p(\tilde{T}|\tilde{A}) = \frac{1}{\sqrt{2\pi}\sigma_{(\ln\tilde{T})}\tilde{T}} \exp\left\{-\frac{1}{2}\left(\frac{\ln\left(\tilde{T}\right) - \ln\left(0.95\tilde{A}^{1.42}\right)}{\sigma_{(\ln\tilde{T})}}\right)^2\right\}, \tag{24}$$

which is conditioned on the gust amplitude $\tilde{A}$ and has a standard deviation of $\sigma_{(\ln\tilde{T})} = 0.6$. The term $\overline{T}$ is the mean gust duration and is computed by the equations

$$\overline{T} = \frac{1}{2N^+(0)}, \quad N^+(0) = \frac{1}{2\pi}\sqrt{\frac{\int_{-\infty}^{\infty}\omega^2 S_{u'u'}(\omega)d\omega}{\int_{-\infty}^{\infty} S_{u'u'}(\omega)d\omega}}. \tag{25}$$

Using a conditional probability density function means, that a great gust needs a longer rise time than a smaller one. As the mean gust duration is a function of the mean wind velocity u_0 it is possible to fit 25 to the function $\overline{T} = 7.998u_0^{-0.2183} - 1.4$, assuming the height $z = 4\,[m]$ and the parameter $z_0 = 0.07$ and integrating from $\frac{1}{600}\,[Hz]$ to $1\,[Hz]$. The high-pass frequency $\frac{1}{600}\,[Hz]$ corresponds to the 10-minute mean wind and the low-pass frequency $1\,[Hz]$ is a typical filter frequency in meteorological measurements, [4].

2.5 Crosswind scenarios

For the calculation of the crosswind stability it is important to determine realistic and reliable wind characteristics. In this work, three different crosswind scenarios, an embankment, a tunnel-exit and a plain turbulent process scenario have been investigated and compared to each other. The artificial gusts are surrogate models for the real turbulent wind characteristic and they are designed to create extreme loads on the railway vehicles.

Embankment-scenario

The so called embankment-scenario is usually used to analyze the response of a railway vehicle on a single gust while operating in constant mean wind conditions. As can be seen in figure 9

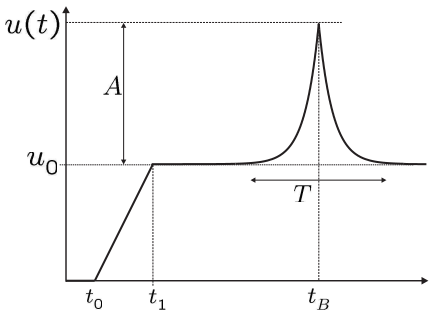

Figure 9: Embankment crosswind scenario

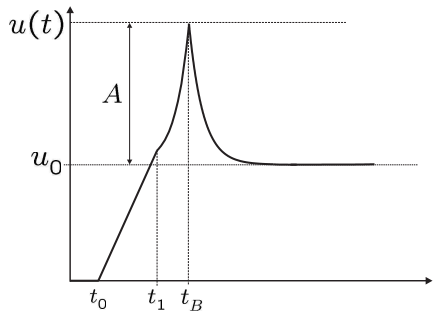

Figure 10: Tunnel-exit crosswind scenario

the wind speed firstly increases linearly from zero to the mean wind velocity u_0 and then after a relatively long time, in which the vehicle oscillations can decay, an exponential gust arises with a certain gust amplitude A at time t_B and a certain gust duration T. The times in figure 9 are defined as $t_0 = 1[s],\ t_1 = t_0 + \frac{L_T}{v_0},\ t_B = t_1 + 13[s] + \frac{T}{8}$ and $t_{end} = t_1 + 13[s] + \frac{T}{4}$, and the linear slope at the beginning is introduced because of numerical reasons, as realistic wind speeds would not increase like that.

Tunnel-exit-scenario

The tunnel-exit scenario is used to investigate the hazard of a sudden gust occurring just after the railway vehicle has left a tunnel or a wind-barrier. Unlike the embankment-scenario the gust is occurring very next to the linear slope and so the wind velocity is rising to the superposition of the mean wind and of the gust wind speed at time t_1. But it is not directly obvious at which time the maximum of the gust shall be. A screening experiment with respect to the gust time t_B has been showing, as can be seen in figure 11 that, for the vehicle model in this work, a gust maximum at time $t_B \approx t_1 + 0.95$ results in a worst case.

Turbulent-process-scenario

The introduced gust models have the inherent problem, that these wind scenarios are artificial designs and therefore do not completely represent a real turbulent wind signal. A fist step in improving the gust models is to add a turbulent signal. As the gust statistics cover the frequency range from $\frac{1}{600}\,[Hz]$ to $1\,[Hz]$ a first approach could be, that the turbulent process should cover higher frequencies. But as the gust scenarios are designed for extreme loads, which have high amplitudes and long rise times, the frequency content of the turbulent signal has been set from $\frac{1}{2T}\,[Hz]$ to $4\,[Hz]$. The upper limit is chosen at $4\,[Hz]$ because of the drastic decay of the aerodynamic admittance function.

As the extreme loads modeled by gust scenarios are part of the normal turbulent PSD, it is straight forward to use the complete turbulent time series as excitation and to simulate the railway vehicle running a long time through this turbulent wind field. As the whole turbulent

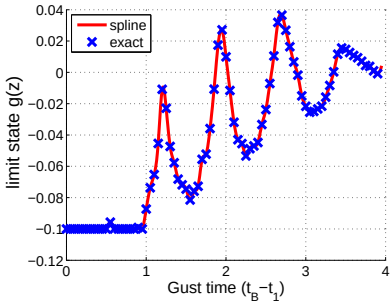

Figure 11: Variation of the limit state function with respect to t_B

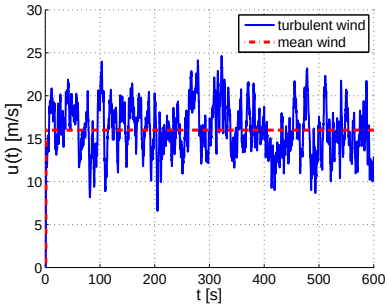

Figure 12: Turbulent wind process

process relies on the 10 minute mean wind and to compare the complete turbulent process with the gust scenarios, the frequency range spans from $\frac{1}{600}\,[Hz]$ to $1\,[Hz]$ and the simulation duration is 10 minutes. A typical velocity signal resulting from a spectral decomposition simulation can be seen in figure 12.

2.6 Wind excitation

After introducing all components of the wind velocity characteristics the resultant excitation has to be formulated. The wind velocity and the railway vehicle are described in two different coordinate systems, as shown in figure 2 and therefore the wind speed has to be transformed to the vehicle fixed $[x_T, y_T, z_T]$-coordinate system. Taking the vehicle velocity v_0 into account the resultant squared wind speed

$$v_{res}^2 = v_0^2 + u^2 + v^2 + w^2 + 2uv_0 \sin\alpha_w - 2vv_0 \cos\alpha_w \tag{26}$$

and the resultant inclination angle

$$\beta_w = \arctan\left\{\frac{|u\cos\alpha_w + v\sin\alpha_w|}{|v\cos\alpha_w - u\sin\alpha_w - v_0|}\right\} \tag{27}$$

can be given. The velocity components v and w will be neglected. For the embankment and tunnel-exit scenarios the averaging

$$\overline{v_{res}^2} = \frac{1}{A_F}\int_{A_F}\left(v_0^2 + u^2 + 2uv_0\sin\alpha_w\right)dA_F \tag{28}$$

of the squared resultant velocity over the vehicle area has to be undertaken, as has already be done for the turbulence by considering the aerodynamic admittance function. Performing the averaging yields

$$\begin{aligned}\overline{v_{res}^2} &= v_0^2 + u_0^2 + [A - u'(t_B)]\,\overline{u_B^{*2}(t-t_B)} + \overline{b_B^2} + 2u_0\,[A - u'(t_B)]\,\overline{u_B^*(t-t_B)} \\ &- 2u_0 b_B + 2\,[A - u'(t_B)]\,\overline{u_B^*(t-t_B)b_B} + 2\left\{[A - u'(t_B)]\,\overline{u_B^*(t-t_B)} - \overline{b_B} + u_0\right\}u'(t) \\ &+ u'^2(t) + 2\left\{u_0 + [A - u'(t_B)]\,\overline{u_B^*(t-t_B)} - \overline{b_B} + u'(t)\right\}v_0\sin\alpha_w.\end{aligned} \tag{29}$$

with the abbreviation $b_B = \frac{\dot{u}_B^*(t-t_B)\dot{u}'(t_B)}{\ddot{u}_B^*(t_B)}$. Not only the wind speed but also the inclination angle β_w has to be averaged. This is done in a simplified manner by not taking the mean of

equation 27 but by utilizing the averaged wind speed over the vehicle area. This results in the mean inclination angle

$$\overline{\beta_w} = \arctan\left\{\frac{\left|\left(u_0 + [A - u'(t_B)]\,\overline{u_B^*(t-t_B)} - \overline{b_B} + u'(t)\right)\cos\alpha_w\right|}{\left|-\left(u_0 + [A - u'(t_B)]\,\overline{u_B^*(t-t_B)} - \overline{b_B} + u'(t)\right)\sin\alpha_w - v_0\right|}\right\}. \tag{30}$$

Because of the inhomogeneous wind velocity over the vehicle area there exists a superelevation of the yaw moment. Especially if the train is coming out of the tunnel or out of the barrier the front part is imposed to the wind whereas the rear part is still in calm conditions. An attempt has been made to approximate this unsteady phenomenon by using the side force definition and a strip approach. The yaw moment $M_{z,\text{total}} = M_z + \Delta M_z$ is split into an averaged part and a variational part, which is calculated by an integration

$$\Delta M_z = \int_{t-\frac{t_T}{2}}^{t+\frac{t_T}{2}} \frac{1}{2}\rho_L \frac{A_F}{t_T} C_{y_T} v_{res}^2(\bar{t}) v_0\,(\bar{t} - t)\,d\bar{t} \tag{31}$$

of the normalized side force times a lever over the whole vehicle area.
Using the derived equations and taking the dependency of the aerodynamic coefficients of the angle β_w into account, it is possible to write down the final equations of the resultant wind forces

$$F_{x_T,y_T,z_T} = \frac{1}{2}\rho_L A_c C_{x_T,y_T,z_T}(\overline{\beta_w})\,\overline{v_{res}^2} \tag{32}$$

and of the resultant wind moments

$$M_{x_T,y_T,z_T} = \frac{1}{2}\rho_L A_c L_c C_{mx_T,my_T,mz_T^*}(\overline{\beta_w})\,\overline{v_{res}^2}, \tag{33}$$

where the yaw moment equation has to be altered as stated above.

3 VEHICLE MODEL

In this paper a characteristic double decker cabin car running with constant velocity on a straight track is simulated in the commercial MBS-Code ADAMS/RAIL. By utilizing this MBS-program it is easily possible to include nonlinear springs and dampers and to model precisely the bump stops of the vehicle. The bump stops are very important because they have a great influence on the overturning behavior of the cabin car. The wheel-rail contacts have been computed by means of Kalker‘s Fastsim algorithm without considering track irregularities.

4 PROBABILISTIC ANALYSIS

Because of the stochastic excitation it is not possible to determine an exact failure boundary (certain wind speed) at which the railway vehicle fails, but it is only possible to compute a probability that the vehicle capsizes. By application of the introduced stochastic embankment wind scenario it is possible to calculate the conditional probability

$$P_G(\underline{z}|u_0) = \int_{\Omega_f} p_Z(\underline{z}|u_0)d\underline{z} \tag{34}$$

that the vehicle fails under the excitation of a single, arising gust while a certain mean wind u_0 is blowing. The tunnel-exit scenario is not included here because it is considered as initial

failure in the proceeding calculations. In equation 34 Ω_f denotes the failure domain which is separated from the save domain by the limit state function $g(\underline{z}) = 0$, and $\underline{z}$ and $p_{\mathrm{z}}(\underline{z}|u_0)$ are the vector of all stochastic variables mapped on the space of standard normal variates and the corresponding probability density functions, respectively. The failure criterion in this case is that the lowest normal wheel force of the railway vehicle is less than 10% of the static normal wheel force.
The expected failure rate is computed by multiplying equation 34 with the occurrence frequency of gusts $N^+(0)$. Under the assumption, that the failure events follow a Poisson process the conditional probability of failure for the time interval $[0, T_f]$ computes to

$$P_{f,T_f}^{u_0} = 1 - P_0 \exp\left\{-N^+(0) P_{G}(\underline{z}|u_0) T_f\right\}, \tag{35}$$

where the probability $P_0 = 1 - P_{f,T_f,\text{tunnel-exit}}$ describes the initial probability of failure by using the results of the tunnel-exit computations, [13].
Using the different approach of independent gust events and under consideration that during the interval $[0, T_f]$ the expected number of gust events is $N^+(0)T_f$, the conditional failure probability

$$P_{f,T_f}^{u_0} = 1 - P_0 \left[1 - P_{G}(\underline{z}|u_0)\right]^{\left(N^+(0)T_f\right)} \tag{36}$$

can also be computed using equation 36. A Taylor series expansion of both expressions 35 and 36 shows identity for the first 2 terms and for small $P_{G}(\underline{z}|u_0)$ both equations will give the same results. The influence of the mean wind can be quantified by integrating equation 35 over the mean wind u_0

$$P_{f,T_f} = \int_{u_{0,d}}^{u_{0,t}} \left(1 - P_0 \exp\left\{-N^+(0) P_{G}(\underline{z}|u_0) T_f\right\}\right) p(u_0) du_0. \tag{37}$$

The probability density function $p(u_0)$ of the mean wind along the track can be taken from meteorological measurements. As normally the measurement stations are not exactly placed at the railroad tracks the mean wind distribution is specified by an averaging process of all surrounding weather stations considering transfer functions from the stations to the track.
The major challenge of the stated procedure is to determine the probability $P_{G}(\underline{z}|u_0)$ for a single gust event, as crude Monte-Carlo simulation is not feasible for high dimensional multi-body systems. To reduce the numerical effort semi-analytical approximations (e.g. FORM) and Monte-Carlo simulations with variance reduction (e.g. Line Sampling) are applied.
For the third wind scenario, the turbulent wind process excitation, a different approach is needed for computing the conditional failure probability $P_{f,T_f}^{u_0}$, as now a time dependent reliability problem with a huge number of important stochastic variables has to be evaluated. A common procedure is to use the theory of extremes and to estimate an extreme value distribution, which then can be used to calculate the probability of failure.

4.1 Semi-analytical approximations

For reliability problems with a relative low number of stochastic variables the Most Probable Point (MPP), which is the point lying on the limit state function with the shortest distance to the origin in the standard normal space, can be determined by the so called First-Order-Reliability-Method (FORM). FORM is directly leading to the optimization task:
Minimize $\sqrt{\underline{z}^T \underline{z}}$ under the condition that the constraint $g(\underline{z}) = 0$ is fulfilled. Using the MPP the

linear approximation

$$P_{G}(\underline{z}|u_0) \approx \Phi\left(-\sqrt{\underline{z}_{MPP}^T \underline{z}_{MPP}}\right) = \Phi\left(-\beta\right) \tag{38}$$

of the conditional failure probability can be given, [14]. The FORM analysis works fine for wind scenarios without turbulence, where maximal seven stochastic variables have been considered.

4.2 Monte-Carlo methods

Utilizing the so called Line-Sampling method an improvement of the FORM results can be given and it is also possible to consider turbulent fluctuations, [7]. Given an important direction $\underline{e}_\alpha$ (e.g. from the FORM analysis), every sample is decomposed perpendicular and parallel to $\underline{e}_\alpha$: $\underline{z}_i = \underline{z}_i^\perp + c_i \underline{e}_\alpha$, where the distance c_i is used to compute the probability $p_i = \Phi(-c_i)$. The probability of failure is then determined by equation

$$P_{G}(\underline{z}|u_0) = \frac{1}{N}\sum_{i=1}^{N} p_i. \tag{39}$$

4.3 Extreme value methods

The extreme value approache can be used to determine the probability of failure $P_{f,T_f}^{u_0}$ of the railway vehicle system under the turbulent wind process excitation. In this work the MAX and the Peak Over Threshold (POT) methods have been utilized. For the MAX method only the n largest values from n independent runs are taken and fitted to the Generalized Extreme Value (GEV) distribution, whereas for the POT method all values above a certain, predefined threshold are taken and then fitted to the Generalized Pareto (GP) distribution. These distributions can subsequently be used to estimate the failure probability, [15].

4.4 Sensitivity methods

The sensitivity analysis investigates the influence of input parameters on the output of a system. It can be distinguished in local and global methods which differ from each other by means of accuracy, computational effort and insight into the system. Local methods are computational less expensive but give also less information about the system and global methods are numerically demanding but give information, averaged over the whole parameter space. Three different sensitivity procedures have been applied to investigate the influence of the stochastic excitation parameters $\underline{z}$ and of the deterministic design parameters.
A semi-analytical, local result can be derived from the previous FORM computations. Differentiating β with respect to $\underline{z}$ and noting that $\underline{z}_{MPP}$ is known yields

$$\left.\frac{d\beta}{d\underline{z}}\right|_{MPP} = \left.\frac{d}{d\underline{z}}\sqrt{\underline{z}^T\underline{z}}\right|_{MPP} = \frac{\underline{z}_{MPP}}{|\underline{z}_{MPP}|}. \tag{40}$$

Using this result the positive sensitivity coefficients $S_i = \frac{|z_{MPP,i}|}{|\underline{z}_{MPP}|}$ can be stated.
To investigate the global influence of the excitation and design parameters the correlation matrix with respect to these variables and concerning the limit state function has been computed and also a principal component analysis concerning the calculated correlation matrix has been undertaken, [16].
A third global method which is less numerically costly than correlation analysis and which gives also a good insight into nonlinearities of the system is the so called Morris-Method. In the

space of all parameters, random walks are performed varying always one factor at a time and computing the finite differences

$$d_i = \frac{g(z_1, \ldots, z_i + \Delta z_i, \ldots, z_n) - g(\underline{z})}{\Delta z_i} \tag{41}$$

with respect to each parameter. The mean values μ_i of the norm of these differences show the global influence of the parameters and the standard deviations σ_i are measures of the nonlinear effects of these parameters.

5 RESULTS

5.1 Reliability analysis

Figure 13 shows the conditional failure probability $P_G(\underline{z}|u_0)$ with respect to the mean wind speed u_0 for driving speeds of $160\left[\frac{km}{h}\right]$ and $200\left[\frac{km}{h}\right]$, respectively. The failure probability varies approximately exponentially with increasing mean wind velocity and as expected, for $200\left[\frac{km}{h}\right]$ the probability is considerable higher. In figure 14 the conditional failure probabilities

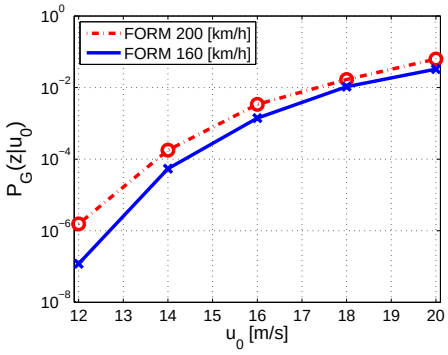

Figure 13: Conditional probability $P_G(\underline{z}|u_0)$ computed by FORM analysis for $160\left[\frac{km}{h}\right]$ and $200\left[\frac{km}{h}\right]$.

u_0	FORM	LS	LS + turbulence
$12\left[\frac{m}{s}\right]$	$1.19e^{-7}$	$1.49e^{-7}$	$2.33e^{-7}$
$14\left[\frac{m}{s}\right]$	$5.41e^{-5}$	$4.12e^{-5}$	$5.26e^{-5}$
$16\left[\frac{m}{s}\right]$	$1.40e^{-3}$	$1.10e^{-3}$	$1.40e^{-3}$
$18\left[\frac{m}{s}\right]$	$1.06e^{-2}$	$9.20e^{-3}$	$1.30e^{-2}$
$20\left[\frac{m}{s}\right]$	$3.28e^{-2}$	$3.58e^{-2}$	$7.46e^{-2}$

Figure 14: Conditional failure probabilities $P_G(\underline{z}|u_0)$ computed by FORM, LS and LS with additional turbulence for $v_0 = 160\left[\frac{km}{h}\right]$.

computed by means of FORM analysis, by Line-Sampling simulation and by Line-Sampling simulation taking additional turbulence into account are presented. The differences between these three analysis methods are not very large and it can be stated that for the investigated railway vehicle the FORM analysis gives reliable results which mostly overestimate the risks. The comparison of the tunnel-exit- and embankment-scenario, as illustrated in figure 15, shows that as expected the tunnel-exit scenario is more critical than the embankment-scenario and translated to mean wind speeds, the difference between both scenarios is about $1\left[\frac{m}{s}\right]$ wind velocity. To reduce this higher overturning risk adequate wind-fences should be placed behind tunnels or barriers. Figure 16 shows the failure probability for a time interval of 10 minutes for different mean wind velocities. The failure probabilities have been calculated by means of extreme value methods (POT and MAX) and by FORM and Line-Sampling simulation consecutively using equation 35 to transfer the FORM and Line-Sampling results to the time dependent problem. The results of these different formularies match quite well for $u_0 \geq 14\left[\frac{m}{s}\right]$, as shown in table 1, but it has to be mentioned, that the computational effort for the POT and MAX models is much higher than the one for the FORM and Line-Sampling analysis. The failure probabilities $P^{u_0}_{f,T_f=600[s]}$ are high and for mean wind speeds of $18\left[\frac{m}{s}\right]$ and more it is almost sure, that the railway vehicle will fail while operating in such strong winds.

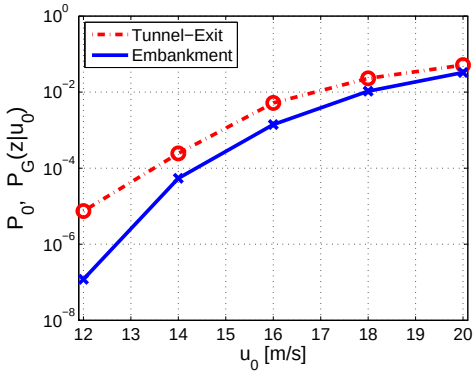

Figure 15: Conditional probabilities P_0 and $P_G(\underline{z}|u_0)$ for tunnel-exit- and embankment-scenario for $v_0 = 160\left[\frac{km}{h}\right]$.

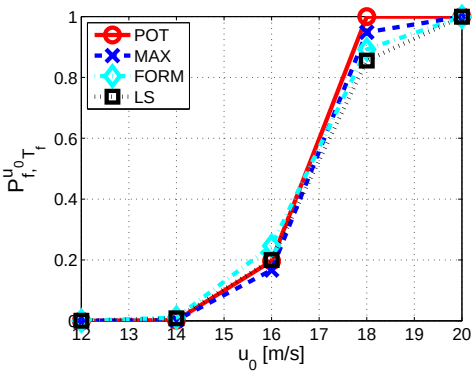

Figure 16: Failure probability $P^{u_0}_{f,T_f=600[s]}$ computed by POT, MAX, FORM and LS methods for $v_0 = 160\left[\frac{km}{h}\right]$.

u_0	POT	MAX	FORM	Line-Sampling
$12\left[\frac{m}{s}\right]$	0.0	0.0	$2.67e^{-4}$	$2.72e^{-4}$
$14\left[\frac{m}{s}\right]$	0.0021	0.0020	0.0107	0.0082
$16\left[\frac{m}{s}\right]$	0.1962	0.1670	0.2468	0.1997
$18\left[\frac{m}{s}\right]$	(3.5968)	0.9486	0.8922	0.8553

Table 1: Failure probability $P^{u_0}_{f,T_f=600[s]}$ computed by POT, MAX, FORM and Line-Sampling simulation for $v_0 = 160\left[\frac{km}{h}\right]$.

5.2 Sensitivity analysis

Local and global sensitivity investigations with respect to the 7 stochastic excitation variables yield the result, that the gust amplitude A, the aerodynamic roll coefficient C_{mx_T} and the

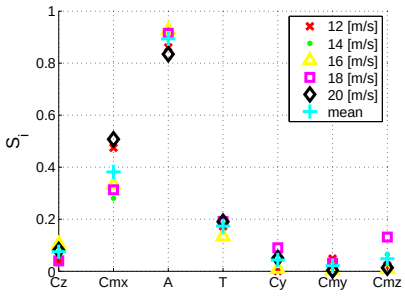

Figure 17: Local gradients of the limit state function $g(\underline{z}) = 0$ at the MPP.

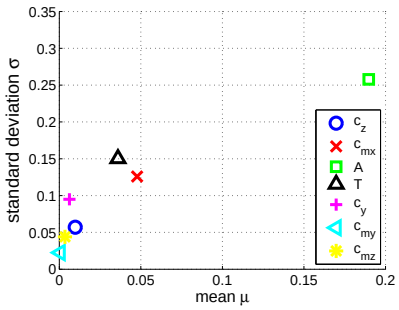

Figure 18: Mean values and standard deviations computed by the Morris-Method.

gust duration T are the most influential parameters, as can be seen in figures 17 and 18. Further investigations (not shown here) have been given the result, that it is sufficient for the calculation of the failure probabilities to consider only these 3 variables and neglecting the others.
Figure 19 shows the impact of several design parameters (antiroll bar (`antiroll`), secondary suspension damper (`SS_Damper`), lateral damper (`LD`), primary vertical damper (`PVD`), primary suspension inner position and outer position (`PS_Cz_in`, `PS_CZ_out`), secondary suspension (`SS_Cz`)) on the limit state function, computed by means of principal component anal-

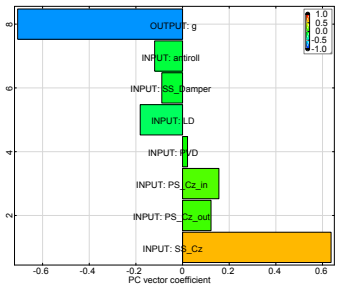

Figure 19: Principal component vector of the design parameters with respect to the limit state function.

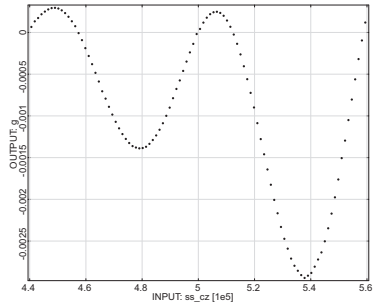

Figure 20: Anthill plot of the limit state function with respect to the linear spring coefficient of the secondary suspension.

ysis. In figure 20 the critical, unwanted, oscillating characteristic of the limit state function concerning the secondary suspension is presented. Relying on principal component results only could in this case lead to wrong results.

6 CONCLUSIONS

In this paper a consistent probabilistic approach for assessing the crosswind stability of railway vehicles is proposed, in which Probabilistic Characteristic Wind Curves (PCWC) have to be computed. The probabilistic properties of the turbulent wind excitation and the uncertainty of the aerodynamic coefficients of the railway vehicle have been considered by stochastic variables which follow certain parametric distributions. The failure probabilities have been computed by means of semi-analytical methods (FORM), by Monte Carlo methods with variance reduction (Line-Sampling) and by using extreme value theory.
The obtained results show, that higher driving velocities increase the failure probability and that the tunnel-exit scenario is clearly more critical than the embankment scenario. Transferred to infrastructural considerations it can be concluded that a smooth increase of the crosswind load on the railway vehicle should be implemented putting adjusted wind-fences along the track. These measures are especially essential for tunnel-bridge combinations in the mountains.
The sensitivity analyses have been performed by means of latin hypercube sampling (LHS) and by subsequent calculations of principal component vectors.
From the seven stochastic variables the most crucial variables have been extracted. The gust amplitude A, the aerodynamic roll moment coefficient C_{mx_T} and the gust duration T have been identified to be most important.
For the design parameters of the railway vehicle such clear results cannot be given. The influences of the considered parameters are, except for the secondary suspension which unfortunately has also an unwanted oscillating functional dependency, quite low.

REFERENCES

[1] 14067-6 prEN: Railway applications-Aerodynamics-Part 6:Requirements and test procedures for cross wind assessment. 2007. – European Standard

[2] BIERBOOMS, W. ; CHENG, P.-W.: Stochastic gust model for design calculations of wind turbines. In: *Wind Engineering and Industrial Aerodynamics* 90 (2002), pp. 1237–1251

[3] CARRARINI, A.: A probabilistic approach to the effects of cross-winds on rolling stock. In: *Proc. European Congress on Computational Methods in Applied Sciences and Engineering*. Jyväskylä, Finland, 2004

[4] DELAUNAY, D. ; LOCATELLY, J.P.: A gust model for the design of large horizontal axis wind turbines: completion and validation. In: *Proc. European Community Wind Energy Conference, Madrid, Spain, pp. 176-180,* 1990

[5] DIEDRICHS, B.: On computational fluid dynamics modelling of crosswind effects for high-speed rolling stock. In: *Journal Rail and Rapid Transit* 217 (2003), pp. 203–226

[6] PROPPE, C. ; PRADLWARTER, H.J. ; SCHUËLLER, G.I.: Equivalent linearization and Monte Carlo simulation in stochastic dynamics. In: *Probabilistic Engineering Mechanics* 18 (2003), pp. 1–15

[7] PRADLWARTER, H.J. ; SCHUËLLER, G.I. ; KOUTSOURELAKIS, P.S. ; CHARMPIS, D.C.: Application of line sampling simulation method to reliability benchmark problems. In: *Structural Safety* 29 (2007), pp. 208–221

[8] SOCKEL, H.: Aerodynamik der Bauwerke. Vieweg Braunschweig Wiesbaden (1984)

[9] COOPER, R.K.: Atmospheric Turbulence with Respect to Moving Ground Vehicles. In: *Journal of Wind Engineering and Industrial Aerodynamics* 17 (1984), pp. 215–238

[10] BAKER, C.J.: Some complex applications of the wind loading chain. In: *Journal of Wind Engineering and Industrial Aerodynamics* 91 (2003), pp. 1791–1811

[11] BEARMAN, P.W.: An Investigation of the Forces on Flat Plates in Turbulent Flow. National Physical Laboratory, NPL Aero Report 1296, april (1969)

[12] BERGSTRÖM, H.: A Statistical Analysis of Gust Characteristics. In: *Boundary-Layer Meteorology* 39 (1987), pp. 153-173

[13] LIN, Y.K.: Probabilistic Theory of Structural Dynamics. McGraw-Hill 1967

[14] LIU, P.L. ; DER KIUREGHIAN, A.: Optimization Algorithms For Structural Reliability. In: *Structural Safety* 9 (1991), pp. 161-177

[15] REISS, R.D. ; THOMAS, M.: Statistical analysis of extreme values. Birkhäuser 2007

[16] LIU, H. ; CHEN, W. ; SUDJIANTO, A.: Probabilistic Sensitivity Analysis Methods for Design under Uncertainty. In: *10th AIAA/ISSMO Multidisciplinary Analysis and Optimization Conference* Albany, New York (2004)